Using Ion-Beam Techniques to Determine the Elemental Composition of ICF Targets

The precise elemental composition of any inertial confinement fusion (ICF) target (capsule, flat foil, or a package attached to a hohlraum) must be known to interpret the results of the implosion. The accuracy of this information was never an issue in earlier experiments: the composition was well known because the targets were straightforward designs (i.e., glass capsules and micro-encapsulated polystyrene shells) that were fabricated using well-characterized polymer chemistry methodologies that yield known compositions. Targets used today are more complicated than those used previously and are fabricated by new methods that are still in their infancy and, accordingly, are less understood.[1] These techniques involve the plasma-induced (a low-temperature, glow-discharge) polymerization of gas-phase monomers. The energy from the plasma and the presence of ions allow gas-phase and gas-surface interactions to occur that are otherwise unattainable using classical solvent chemistry because numerous reaction mechanisms are now thermodynamically and kinetically allowed. The resulting materials are amorphous solid-state solutions where the composition cannot be inferred *a priori* from the processing conditions. The overriding importance of this target-fabrication technique, however, is that thin-wall capsules, and capsules with discrete radial regions of the capsule wall doped with mid- to high-atomic-weight elements, can now be produced.[2] The associated uncertainty regarding the composition of these targets now requires the evaluation and application of suitable analysis techniques.

When a target is made of commercially available material, the material assay is accurately known. When targets are made using coating processes, only the composition of the source (precursor) material is well known; independent analysis of the as-deposited material is needed if the composition is to be accurately known. This analysis is done by many methods: The most common technique is electron microscopy using either energy-dispersive or wavelength-dispersive x-ray detection to identify the elements. These techniques are well established, and quantitative data can be obtained with the use of NIST standards. The diagnostic probe size is small (typically <1-μm diameter, 5 μm deep) and nondestructive, features that are desirable for analyzing ICF targets. Another technique adapted for ICF-sized shells—x-ray fluorescence—is also nondestructive and is used to identify dopants (chlorine, titanium, germanium, silicon) in individual shells according to their characteristic x-ray emission signal.[3] Carbon, hydrogen, oxygen, and nitrogen cannot be detected. Again, the actual elemental composition can be quantified if a suitable external calibration of the technique can be established. The techniques discussed here provide a third nondestructive method for assaying individual capsules, with the added virtue that they do not require external calibration. This eliminates several sources of uncertainty in the measurement.

In this article the capabilities and limitations of the ion-beam techniques along with the accuracy that can be achieved in the absence of external calibration are discussed. An analysis of current ICF capsules and some flat-foil targets is presented. This is not the only work that has used ion-beam techniques to characterize ICF targets: recently, Sandia National Laboratory reported on using ion tomography to measure the density and density uniformity of foam targets used in Sandia's ICF program.[4]

Rutherford Backscattering Spectroscopy

The first of two ion-beam techniques used to determine the elemental composition of ICF targets is Rutherford backscattering spectroscopy (RBS). This technique analyzes the energy of ions elastically recoiled off a surface. The stoichiometry, areal density, and presence of impurities in the top 5 to 20 μm of the material can be absolutely determined. Elements with atomic number $Z \geq 4$ can be identified at concentrations as low as 100 parts per million (the sensitivity depends on the atomic mass of the elements involved). The typical surface area of the analysis beam is 1×1 mm, although smaller probe dimensions (limit: 1-μm diam) are achievable by using quadropole electro-optics to focus the beam. The principal disadvantage of the RBS technique is that it cannot be used to detect elements at trace concentrations: it has moderate sensitivity to heavy elements in mid- to light matrices (threshold is 1 in ~10^4) and poor sensitivity to light elements in heavy matrices (threshold

~1 part in 10). Fortunately, these limitations do not apply to the ICF targets investigated for this article. A second limitation of the RBS technique is the logistical one of having ready access to the equipment. The equipment is expensive to purchase and operate and exists only in a few universities and commercial organizations.

RBS also quantifies the composition of the film at varying depths: the minimum resolvable depth increment is 5 to 10 nm, and the maximum depth the technique can probe depends on the material composition of the film and the ion beam. For example, a He$^+$ beam at 2.0 MeV can distinguish chlorine in a hydrocarbon matrix to a depth of ~6 μm; a H$^+$ beam at 1.4 MeV can distinguish chlorine in the same polymer down to 20 μm. These capabilities allow the location and concentration of dopants in a multilayered polymer capsule to be accurately characterized. (A concern in the fabrication process is that the dopant may diffuse out of its original layer when the capsules are processed after the vapor-phase, plasma-polymerization process is complete.)

Principles

Analysis ions are accelerated to a well-defined energy (typically 1 to 10 MeV) and are focused onto the target. Most ions lose energy through inelastic collisions with the target substrate and are implanted into, or are transmitted through, the substrate. A very small fraction of the incident ions elastically recoil off atoms in the target substrate, and a further fraction of the recoiled ions have sufficient energy to escape from the solid and be detected. The energy of the recoiled ions is measured using a surface-barrier detector, and the number of ions in a predefined energy range (referred to as a channel) is counted. The substrate atoms are identified by measuring the energy of the recoiled atom, allowing for the energy the ion loses traversing (both entering and exiting) the substrate. The number of atoms per cross-sectional area is determined from the total number of recoils detected.

A schematic representation of the recoil process is shown in Fig. 75.14(a), and the resulting backscattered spectrum, in Fig. 75.14(b). The abscissa displays the energy of the recoiled ions, where the bandwidth of each energy channel is the energy resolution of the detector (16 keV) and the highest channel number has the greatest energy. The abundance and distribution of elements A and B are calculated from the peaks A_A and A_B. The peak height depends on (1) the absolute number of identical substrate atoms at each resolvable discrete depth and (2) the kinematics of the ion–atom interaction. The peak width

depends on the distribution of the identical substrate atoms through the film depth: ions that recoil from deeper within the solid possess lower recoil energies as they lose energy traversing the substrate. The ratio of the energy E_0 of the incident ion to the energy E_1^A of the high-energy side of peak A is the kinematic factor $K_A = E_1^A / E_0$, which is specific for the incident ion, the target atom, and the scattering angle. The kinematic factor is also given by

$$K = \left\{ \left[\left(M_2^2 - M_1^2 \sin^2 \theta \right)^{1/2} + M_1 \cos \theta \right] \Big/ \left(M_1 + M_2 \right) \right\}^2 ,$$

where θ is the laboratory angle through which the incident ion is scattered and M_1 and M_2 are the masses of the incident ion and target atom, respectively.[5] K, M_1, E_0, and θ are all known, allowing M_2 to be determined. (It is physically intuitive that the greater the mass of the substrate atom, the higher the energy of the recoiled He ion.) The physical basis for this equation is that the kinematic factor depends on the conservation of energy and momentum in a two-body collision, a realistic approximation at these energies (0.5 to 5 MeV for He$^+$) where the collisions are pure Coulombic and where relativistic and off-resonance nuclear reactions do not occur. Tables of the kinematic factors are available for many incident ions (including ^{1}H$^+$ and ^{4}He$^+$) and substrate atoms at discrete recoil angles (θ).[5] An added significance of the kinematic factor is that it influences the mass resolution of the technique; the incident ion and ion energy can be varied to resolve elements with similar masses. Other important factors affecting the accuracy and sensitivity of the technique are the resolution of the surface-barrier detector and energy straggling by the ion beam as it penetrates into the surface (i.e., statistical fluctuations that cause the initially monoenergetic ion beam to assume an increasingly wide energy range as the penetration depth increases).

The areal density of the ith element is determined from the knowledge of the experimental configuration [Fig. 75.14(a)]: the detector solid angle Ω; the integrated peak count A_i, for a known number of incident ions Q; and the measured, or calculated, cross section $\sigma_i(E, \theta)$:

$$N_i \, t = \frac{A_i \cos \theta}{Q \Omega \sigma_i (E, \theta)},$$

where N_i is the atomic density of the ith element and t is the film thickness. If the scattering is Rutherford, the cross section $\sigma(E, \theta)$ can be calculated:

$$\sigma(E,\theta) = \left(Z_1 Z_2 e^2 / 4E\right)^2$$

$$\times \frac{4\left[\left(M_2^2 - M_1^2 \sin^2 \theta\right)^{1/2} + M_2 \cos\theta\right]^2}{M_2 \sin^4 \theta \left(M_2^2 - M_1^2 \sin^2 \theta\right)^{1/2}},$$

where Z_1 and Z_2 are the atomic numbers of the incident ion and target atom, respectively, and $e^2 = 1.44 \times 10^{-13}$ MeV-cm.

This analysis typically yields ±3% uncertainty for the areal density measurement and less than 1% uncertainty for the average stoichiometry. This precision decreases as deeper layers are analyzed because of energy straggling.

Material analyses using these techniques are typically done with ^{4}He ions and modest accelerator energies (0.5 to 2 MeV). At higher and lower energies, the elastic-scattering cross section departs from the Rutherford cross section (i.e., near Coulombic): at lower energies the deviation is due to the nuclear charges being partially screened by the electron shells of both nuclei; at higher energies the deviation is caused by the presence of short-range nuclear forces. Helium is typically used because the backscattering cross sections with all atoms larger than beryllium are nearly Rutherford in this energy region, and there is extensive experimental data regarding the kinematic factors and Rutherford-scattering cross sections.

Nuclear Resonance Analysis of Hydrogen

Accurately quantifying the amount of hydrogen in materials is extremely difficult. Most analytical techniques are unable to detect hydrogen. Those that can detect hydrogen quantify the atom indirectly by probing those atoms/complexes that incorporate hydrogen, i.e., classical spectroscopy looks at the absorption/emission of hydrogen-bonded complexes; electron-detection–based techniques (i.e., x-ray photoelectron spectroscopy and electron-energy-loss spectroscopy) quantify hydrogen from the electron-energy-loss spectrum. More conventional methods (i.e., combustion analysis) that can quantify the hydrogen content typically require a large sample size. This introduces an additional source of uncertainty when analyzing ICF targets since many (typically in excess of 100) capsules are required to obtain the necessary mass. The measured hydrogen content is thus an aggregate value that averages several processing batches and many capsules from the same batch. Consequently, it is impossible to know how much the hydrogen content varies from one target to the next.

Ion-beam–based techniques have been used for more than 10 years to measure hydrogen concentrations in thin films. Because these techniques are sensitive to small variations in hydrogen concentrations and require only a small sample size, they are convenient for analyzing ICF targets. Two ion-beam techniques exist: One technique, elastic recoil detection (ERD), is the reverse of classical RBS since heavy incident atoms forward-scatter lower-Z substrate atoms ($1 \leq Z \leq 9$) and are themselves kinematically recoiled.[5] The second technique is

(a)

(b)
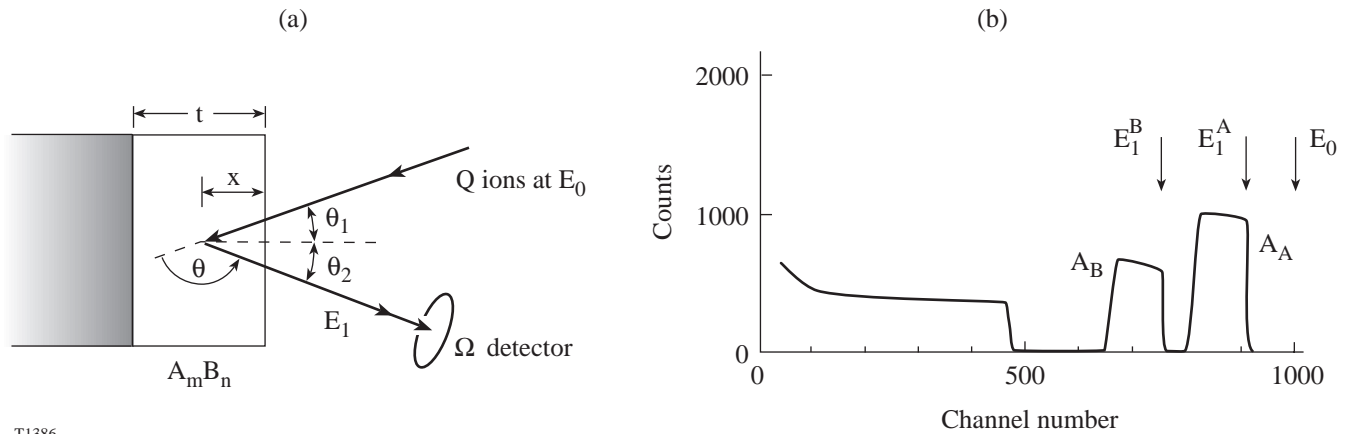
T1386

Figure 75.14

(a) Schematic of the experimental geometry used for RBS. (b) Associated Rutherford backscattered spectrum for a two-element material ($A_m B_n$) on a lower-mass substrate.

nuclear resonance analysis (NRA). This technique measures the gamma-ray product (γ) of a nuclear reaction[5]

$$^{15}N^{++} + {}^{1}H \rightarrow {}^{12}C + {}^{4}He + \gamma\,(4.43 \text{ MeV}).$$
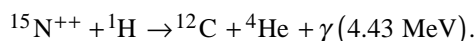
The reaction cross section at the resonance energy (6.385 ±0.005 MeV) is large and decreases rapidly off resonance; the cross section is four orders of magnitude lower and 8 keV off resonance. The γ-ray yield is proportional to the hydrogen concentration at the resonant energy and is accurate to within 2 at.%. Depth profiling is achieved by varying the incident $^{15}N^{++}$ energy, and as the ion loses energy traversing the solid, a region develops within the solid where the ion energy is at resonance (6.385 MeV) and γ rays are produced. The detection "window" equates to a depth of ~7.5 nm in the solids analyzed for this article. This technique's advantage over ERD is greater depth resolution and sensitivity, and it is this latter technique that is used to analyze ICF targets.

Experimental Conditions

The ion-beam work was analyzed using the Dynamitron Accelerator (Model P.E.A.-3.0) at the Accelerator Laboratory at the State University of New York at Albany. The three ions used were $^{1}H^{+}$, $^{4}He^{+}$, and $^{15}N^{++}$ at energies of 1.4, 2, and 8 MeV, respectively. Three beamlines were used. One beamline was configured for standard RBS analysis (nominal 1-mm × 1-mm spot size). The laboratory geometry [Fig. 75.14(a)] was as follows: the angle between the beam and the detector, ($\theta_1 + \theta_2$), was 14°; the angle between the sample normal and the detector, θ_2, was 7°; the sample normal was 7° above the equator; and the solid angle Ω of the surface-barrier detector was 31 msr. The second beamline was configured for microprobe analysis (spatial spot size ~1-μm diam); the detector was above the incoming beam at $\theta_1 + \theta_2 = 23°$; the sample was perpendicular to the beam; and the solid angle was 87 msr. The third beamline used $^{15}N^{++}$ for hydrogen analysis. A NaI scintillation detector was positioned directly behind the incident ion beam.

Data recorded during the 5 to 10 min typically required to acquire a RBS spectrum are (1) the number of recoils at each discrete energy resolvable by the surface-barrier detector (FWHM resolution is 16 keV); (2) the total current and charge striking the target; and (3) a correction for the dead time of the pulse-height analyzer. The total charge and current incident on the surface were optimized to obtain a satisfactory signal-to-noise ratio while minimizing any ion-beam damage to the substrate. This latter effect is of special concern as most of the

analyzed materials are plastics and are susceptible to bulk heating effects. Typically the total charge delivered to the substrate is less than 10 μC/cm^2. This threshold was chosen based on a related report that found that bombarding a teflon film with 6-MeV nitrogen ions decreased the fluorine concentration by only 1%.[6] Since carbon–hydrogen and carbon–fluorine bonds have comparable strengths, this ion-beam threshold is believed to have a minimal perturbation on the target's composition. This was confirmed by measuring the hydrogen content of solution-cast polystyrene films to be 50 at.%, the theoretically expected value. The total dead time of the detector is kept below 10% by controlling the ion-beam current. Finally, particle-induced x-ray emission (PIXE) data were acquired and used to help qualitatively identify the elements present in the material.

Data Analysis

The first step to determine whether ion-beam techniques are suitable for analyzing ICF targets is to calculate the behavior of an energetic ion in an ICF target. Of interest are the trajectory and penetration range of different ions, at specific energies, within the material. These data are available using "Stopping and Range of Ions in Materials"[7]—a software that uses the known collisional cross sections and stopping powers to perform a Monte Carlo simulation of an ion's path through the material. In this manner the divergence ("straggling") of the beam as a function of depth can be determined. Also, the energy lost by the ion to the substrate as it penetrates deeper into the material can be determined.

An example of this simulation is shown in Fig. 75.15. The modeled substrate is a multilayered polymer capsule, as provided by General Atomics, and analyzed by RBS (Fig. 75.16). The incident He ion is at 2 MeV and is defined as a point source on the surface of the substrate. The ion penetrates 9.44 μm into the plastic with a depth "straggle" of 0.18 μm and a radial divergence of ~0.3 μm [Figs. 75.15(a) and 75.15(b)]. Figure 75.15(c) shows the energy lost as a function of depth as the He ion penetrates the material; on average, the ion loses ~20 eV/Å. This information is useful for determining whether the ion beam is heating and possibly altering the substrate. These data confirm that a microprobe beam with a 2-μm-diam spot size will sample a cylindrical volume no greater than 3 μm in diameter and ~8 μm deep.

The Rutherford backscattering spectrum is analyzed using a standard code—Rump[8]—which uses known kinematic factors, Rutherford cross sections, and stopping powers to simulate a backscattered energy spectrum for any material

composition. The procedure is to first simulate the RBS spectrum using a "guessed" elemental composition and then compare the theoretical spectrum with the actual spectrum. The guessed composition is then refined and the theoretical spectrum recalculated. The process is iterated until the stimulated recoil spectrum corresponds with the actual spectrum. When the material is not isotropic, it is necessary to specify the composition of the material at discrete layers. Agreement between the theoretical and actual spectra of various ICF polymer targets is shown in Figs. 75.16–75.18. The accuracy of these analyses is ±2 at.% of the absolute value for the primary

components (i.e., C, N, O) and 5% to 20% for trace (<10 at.% total concentration) dopants such as Cl, Si, Ge, and Ti.

RBS detects elements with atomic numbers greater than 4. As this excludes hydrogen, a major component of ICF polymer capsules (~50 at.%), its concentration was determined using nuclear resonance analysis. The hydrogen concentration (ρ_H) is related to the experimentally measured gamma-ray yield (Y) by

$$Y = \int Q\rho_H(x)\sigma(x)\,dx,$$

(a)
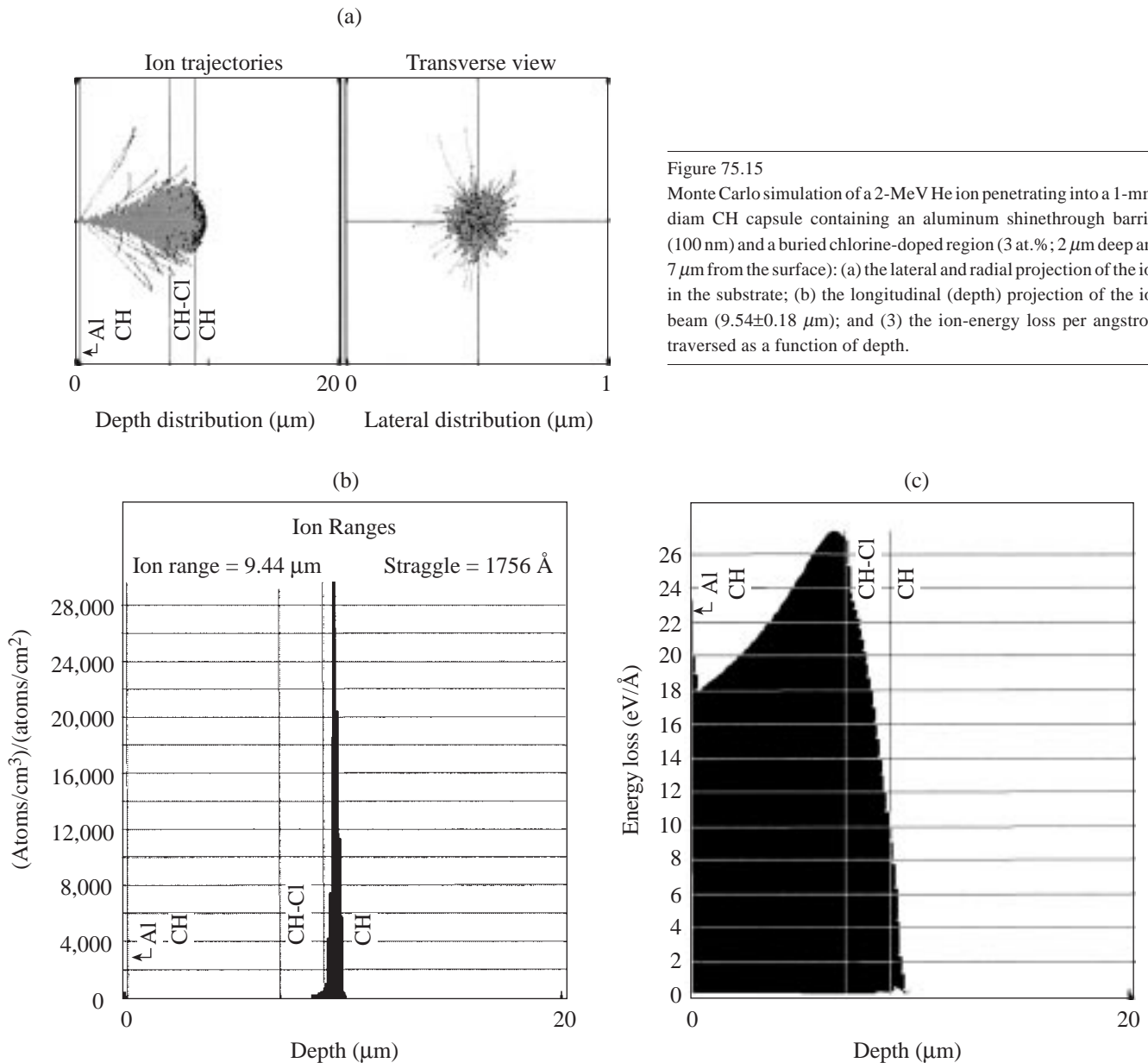
Figure 75.15
Monte Carlo simulation of a 2-MeV He ion penetrating into a 1-mm-diam CH capsule containing an aluminum shinethrough barrier (100 nm) and a buried chlorine-doped region (3 at.%; 2 μm deep and 7 μm from the surface): (a) the lateral and radial projection of the ion in the substrate; (b) the longitudinal (depth) projection of the ion beam (9.54±0.18 μm); and (3) the ion-energy loss per angstrom traversed as a function of depth.

(b)

(c)

T1420

where Q is the number of incident ions and σ is the cross section. Clearly, this cross-sectional dependency requires the film's elemental composition (elements other than hydrogen), film thickness, and density to be accurately known—information that is obtained from the RBS analysis.

Using $dx = dE/(dE/dx)$ gives

$$Y = Q\int \frac{\rho_H(E)\,\sigma(E)}{dE/dx}\,dE,$$

where

$$\sigma(E) = \frac{\sigma_0 \Gamma^2/4}{(E - E_{res})^2 + \Gamma^2/4}$$

is the Breit–Wigner formula,[5] σ_0 is the cross section at the resonance energy, and Γ is the full width at half-maximum of the cross section. Integration yields

$$Y = \frac{Q\rho_H \pi/2\sigma_0\,\Gamma}{dE/dx}$$

or

$$\rho_H(x) = K(dE/dx)Y(x),$$

where K is a constant incorporating all the cross-section parameters (including detector efficiency). K is independent of the material being analyzed; for example, to calculate the amount of hydrogen in a hydrocarbon:

$$\rho_H(\text{at.\%}) = (0.45 \times 10^{19})(dE/dx)_{CH}$$
$$(\text{measured \# counts}/\ 0.5 - \mu C\ \text{total charge}),$$

and

$$(dE/dx)_{CH} = \rho_{CH}\frac{\chi_C(dE/dx)_C + \chi_H(dE/dx)_H}{\chi_C MW_C + \chi_H MW_H},$$

where 0.45×10^{19} is the constant K, dE/dx is the stopping power of the CH substrate, MW is the molecular weight, and χ is the atomic fraction. The penetration depth is equal to

$$\left[E(^{15}N) - E_{reson}(6.385\ \text{MeV})\right]/(dE/dx)_{CH}.$$

Clearly, to completely analyze a polymer capsule, both RBS and NRA data sets must be obtained and iterated until each data set can be accurately simulated with the same elemental composition.

Results

1. Plasma Polymer Capsules

The elemental composition of all types of ICF capsules used at LLE are summarized in Table 75.III. For the most common type of ICF target, a hydrocarbon capsule made by plasma
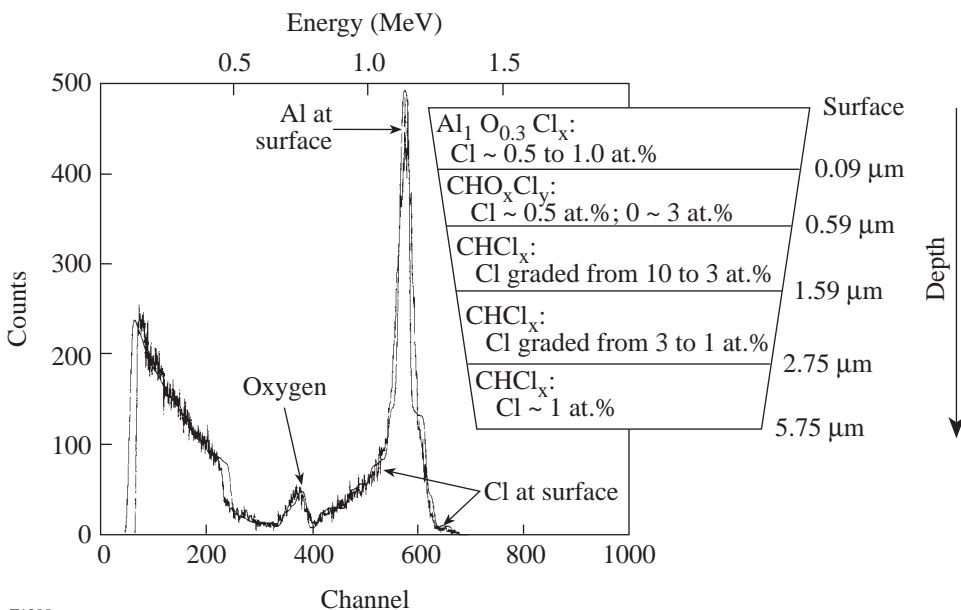
Figure 75.16
RBS spectrum of a 900-μm-diam capsule overlaid with the simulated spectrum. The Cl distribution of elements in the top 5.75 μm is inset.

T1285

Table 75.III: The range of composition of each element in capsules and flat films provided by GA, as measured using ion-beam analysis.

Film Material	Composition (fractional-atom content)						
	Carbon	Hydrogen	Silicon	Germanium	Titanium	Chlorine	Oxygen
CH	0.4→0.48	0.5→0.55					0.02→0.06
CH-Cl	0.44→0.47	0.50→0.53				<0.01→0.1 (pyrolyzed) 0.02→0.03 (unpyrolyzed)	0.01→0.04
CH-Ti	0.33→0.43	0.42→0.62			0.015→0.067	0→0.015	0.02→0.08
CH-Si	0.40	0.47	0.06				0.07
CH-Ge	0.42→0.44	0.48→0.50		0.02→0.04			0.02→0.08

polymerization, the hydrogen concentration ranged from 50 to 55 at.%. There is insufficient data to determine statistically if this variation is inherent in the plasma-processing method or if the fluctuation is a measure of the repeatability of the process. Oxygen was also identified in the polymer; the quantity varied from <1 at.% to a maximum of ~6 at.%. It is speculated that oxygen is adsorbed from the environment and that the concentration depends on how long the capsule was exposed to air. (The maximum of 6 at.% was observed after the plastic had been stored in the laboratory for several months.)

Data obtained from analyzing capsules doped with high-atomic-number elements are summarized below.

a. Silicon-doped capsules. The concentration was constant at 6±1 at.% in all the shells and flat films analyzed. Moreover, silicon was uniformly distributed throughout the depth of the shell wall, as far as the ion beam could probe (6 μm). Figure 75.17 (spectrum 3) shows that the leading edge of the silicon signal was suppressed when a hydrocarbon plastic overcoat was applied (as was expected). Importantly, this signal remained suppressed when the capsule was pyrolyzed (a necessary processing step to remove the mandrel). The absence of any signal due to silicon having diffused to the outer surface of the capsule demonstrated the thermal stability of the silicon-doped plastic; hence, this material is suitable for processing by the current target-fabrication techniques. The oxygen content was 7 at.%.

b. Germanium-doped capsules. The germanium-doping fabrication process was evaluated by examining Ge-doped capsules made simultaneously in the same batch and also in different batches. As with the silicon-doped capsules, the germanium concentration was uniformly distributed throughout the wall of the capsule (shown in Fig. 75.18), and oxygen was present. The measured germanium concentrations varied from 2 to 4 at.% from one capsule to the next. The variation is a measure of the repeatability of the processing conditions: plasma polymer capsules fabricated at the same time varied by less than <1 at.% while those made in different batches varied by a factor of 2. Although the processing conditions were intentionally identical for all the batches analyzed, the varying germanium concentrations demonstrate the inherent control and repeatability of the process.

c. Titanium-doped capsules. The ion-beam analysis technique was used by LLE to assist GA in developing Ti-doped plasma polymer capsules. Capsules were produced using purposely varied processing parameters, and the resulting titanium concentrations varied from 1 to 8 at.%. High titanium concentrations (6 at.%) were accompanied by high oxygen levels (9 at.%) and lower hydrogen concentrations (41 at.%). Figure 75.19 shows this correlation; the depth-profiled hydrogen concentrations at 0.1, 0.28, and 0.44 μm are shown for two films containing different titanium concentrations. Currently, capsules with titanium concentrations of from 3 to 6 at.% are available.

d. Chlorine-doped capsules. The chlorine content was analyzed using both helium and hydrogen ion beams; the former provided greater sensitivity and accuracy while the latter provided greater penetration that allowed the complete 20-μm wall of the capsules to be profiled. The quantity and position of the chlorine were found to be strongly dependent on
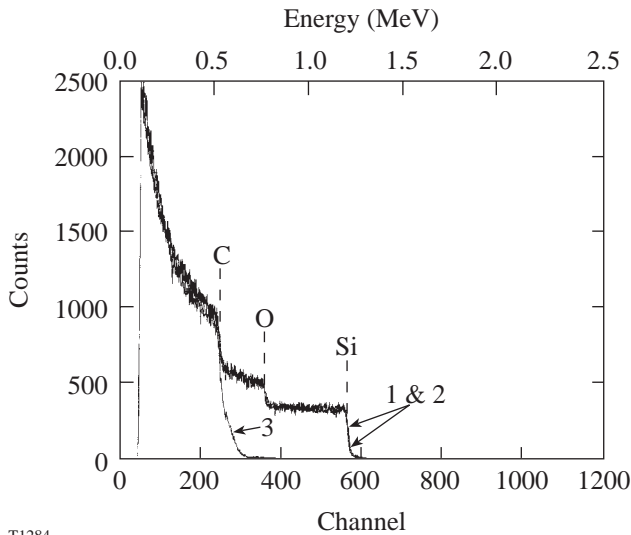
T1284

Figure 75.17
RBS spectra of three silicon-doped capsules show that the silicon is uniformly distributed through the capsule wall and is thermally stable: (1) Si-doped CH; (2) Si-doped CH after pyrolysis; and (3) Si-doped CH overcoated with CH and then pyrolyzed at 300°C.
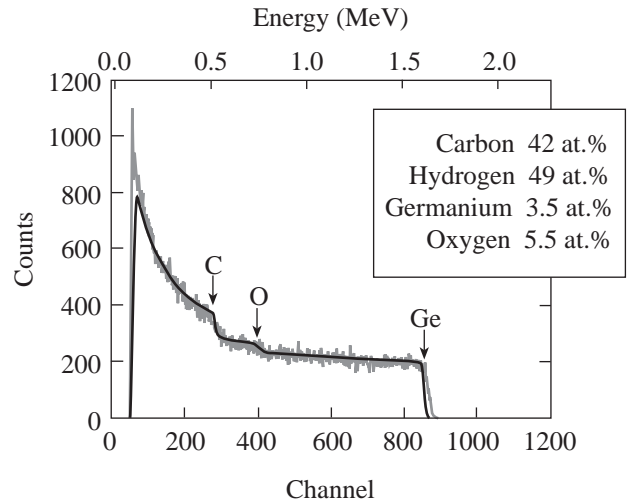
T1387

Figure 75.18
RBS spectrum of a Ge-doped capsule. Germanium is uniformly distributed through the first 5 μm of the capsule wall.
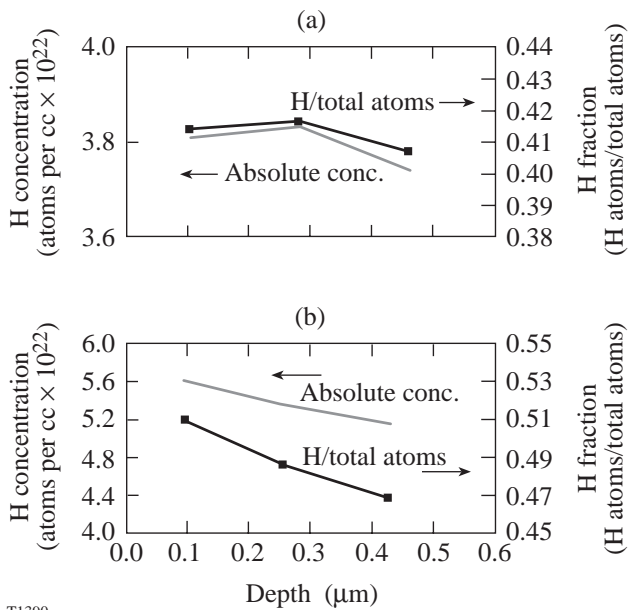
T1390

Figure 75.19
Depth-profiled hydrogen concentrations (expressed as an absolute density and an atomic fraction) in two Ti-doped plastic films: film (a) consists of 44-at.% carbon, 6-at.% titanium, and 9-at.% oxygen content, and film (b) consists of 42-at.% carbon, 2-at.% titanium, and 6-at.% oxygen.

how the polymer capsule was processed. When the capsule was pyrolyzed at 300°C after fabrication (as is typically done to remove the decomposable mandrel), chlorine diffused from the originally doped layer and was distributed throughout the shell wall. The chlorine concentration at any depth would vary from <1 to 10 at.%, with the higher concentration measured in a very thin band at the external wall of the shell. The distribution is shown in Fig. 75.16. Here, chlorine was intended to be located in a 2-μm region 7 μm beneath the surface. In reality, chlorine was detected throughout the top 5.75 μm of the capsule—the maximum depth at which the He ion at 2 MeV could detect chlorine in plastic. A hydrogen ion beam was used to extend the depth sensitivity to detect how far chlorine had diffused into the capsule's wall (a different capsule from the one analyzed above). The resulting spectrum is shown in Fig. 75.20. The chlorine-doped layer was intended to be 1 μm thick and 6 μm below the surface with a concentration of 6 at.%. Actually, the layer was distributed through the top 10 μm of the capsule with an average concentration of 0.05 at.%; no chlorine was detected at greater depths.

Analysis of many chlorine-doped capsules shows the chlorine concentration to be 2 to 3 at.% and thermally stable when the chlorine-doped layer is deposited after the pyrolysis is complete. The consequence of these results for designing targets for ICF experiments is that capsules with a chlorine-doped layer within 3 μm of the inner surface are not achievable; conversely, capsules with a chlorine-doped layer more than 3 μm from the inner surface are feasible.

Energy (MeV)
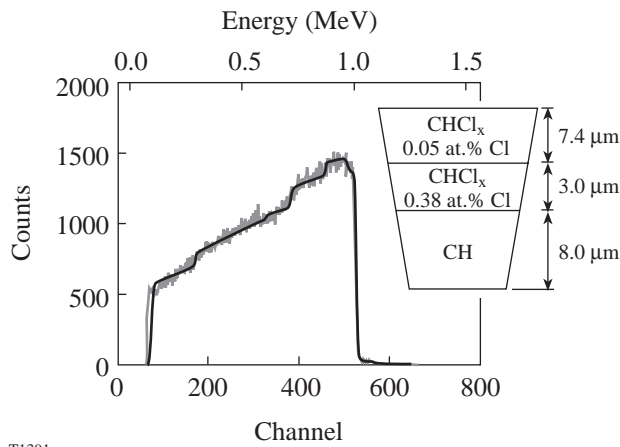
T1391

Figure 75.20
The experimental RBS spectrum of a Cl-doped CH capsule overlaid with the simulated fit. A 1.4-MeV H-ion beam profiled the entire 18.4-μm thickness of the capsule wall.

e. *Deuterated capsules.* The fully deuterated polymer capsule is an important type of ICF target. It is made by polymerizing deuterated-gas monomers onto a poly-α-methylstyrene mandrel and then pyrolyzing the composite to remove the mandrel. It is important that no hydrogen be present in the capsule wall after the process. [It is possible that the deuterium in the CD wall and the hydrogen in the poly-α-methylstyrene (PAMS) wall could exchange during the pyrolysis process.] Hydrogen was not detected in the CD capsule wall, which, given the threshold sensitivity of the NRA technique, limits the hydrogen content in the deuterated plastic to be below 1 at.%.

2. Flat-Foil Targets

A type of target used in plasma physics experiments consists of several layers of different elements used to spectroscopically diagnose the plasma temperature. The more accurately the number of atoms in each layer is known (from the measured film thickness, composition, and areal density), the more accurate is the temperature measurement.[9] Current sputter-deposition and evaporation techniques measure the deposition rate using quartz crystal monitors, a method that can measure the film thickness to within 3%–8% but cannot measure the elemental composition. An independent nondestructive method for analyzing targets after they are assembled is needed, and RBS is a suitable technique.

A target analyzed here consisted of a 1-mm-diam plastic (CH) film overcoated with two thin layers of Ti and KCl. The thickness was measured with 3% accuracy. The titanium layer consisted of 30-at.% oxygen (not surprising since titanium is an effective oxygen getter), and the stoichiometric ratio of K to Cl was 1 to 1. These data allowed the total number of titanium, potassium, and chlorine atoms to be determined.

A type of target used for hydrodynamic instability studies uses an open-cell foam (2- to 5-μm pore size; 1-mm diam and 100 μm thick) overcoat to help minimize the growth of the Rayleigh–Taylor instability. Whereas the target design called for a thin, gold overlayer on the foam, fabrication complexities made it impossible to ensure that the gold was confined to the foam's outer surface (given the open cell structure of the material). The RBS spectrum determined that the sputtered gold atoms had penetrated 30 μm below the surface (Fig. 75.21). These data demonstrated that the target, as-

Energy (MeV)
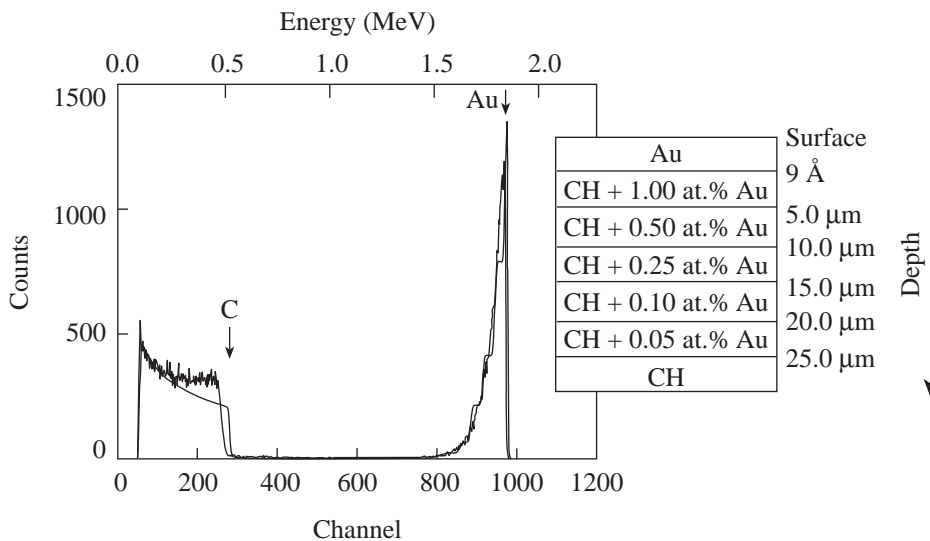
T1421

Figure 75.21
The experimental and simulated RBS spectra of a 30-mg/cm^3-polystyrene foam overcoated with 1 nm of gold.

fabricated, differed significantly from what was intended. This information helps define the capabilities and limitations of different target-fabrication methodologies, which is essential for building new types of targets.

3. Polyimide Shells

The ion-beam analysis technique has also been used to assist the polyimide-shell-development effort.[10] Compositions of films deposited by different processing conditions were determined using both RBS and NRA. Examples of the depth-profile data are shown in Fig. 75.22. These data show that both the elemental ratio in the polyamic acid precursor and the resultant polyimide material were very close to the expected

stoichiometric values; however, both materials possessed excess nitrogen (~2 at.%). This information has allowed the processing parameters to be refined with the goal of optimizing the mass flux of the two precursor monomers.[11]

As discussed previously, RBS provides areal density information, and additional information about the actual (theoretical or measured) density is required to extract the film-layer-thickness information. Conversely, if the film thickness is known, then the actual density can be determined. This approach was used to determine the density of the precursor (polyamic acid) and final (polyimide) films. Films of measured thickness were analyzed, and the density of the

T1388,89
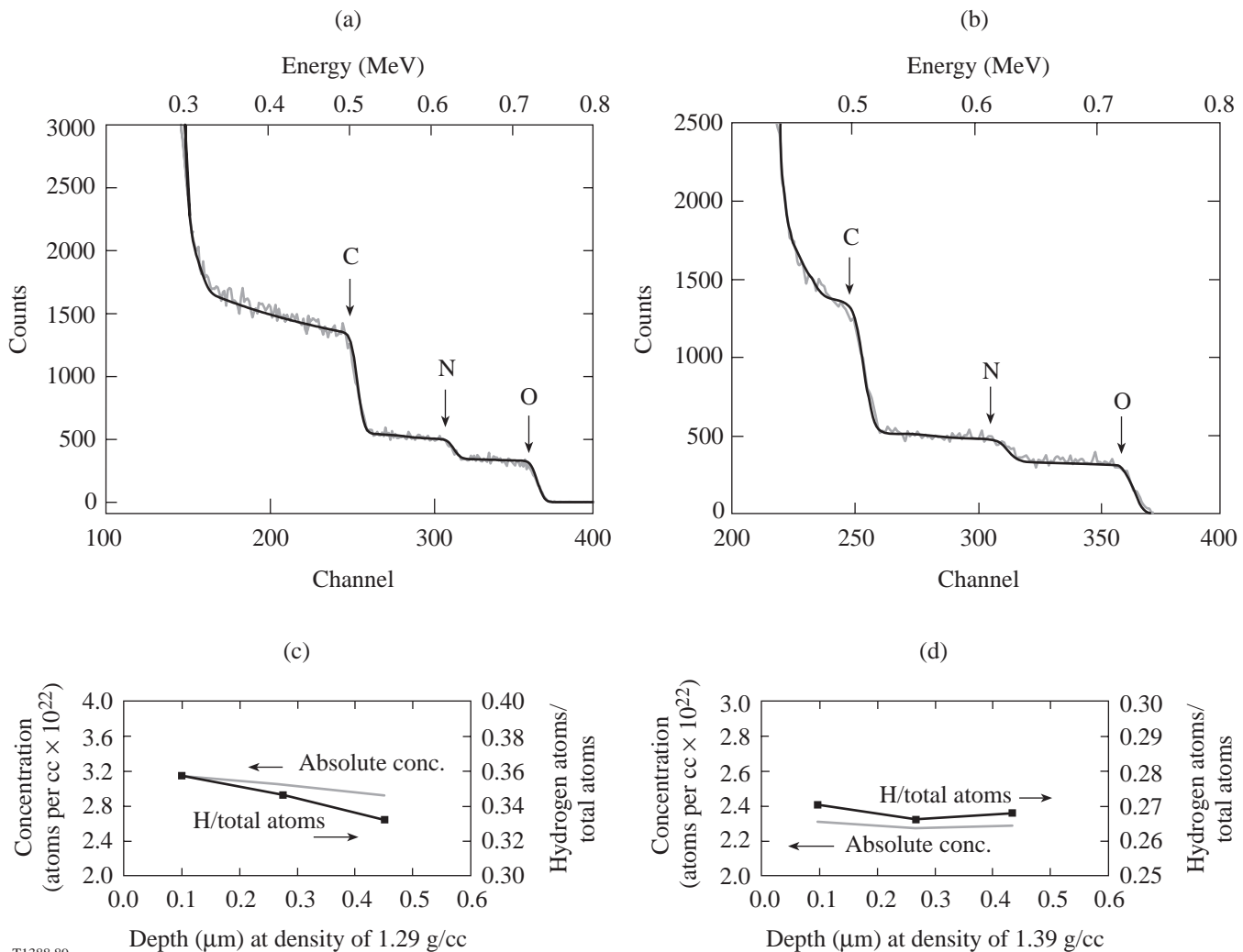
Figure 75.22
The experimental RBS spectra (with the simulated spectra overlaid) and NRA spectra of polyamic acid [(a) and (c)] and polyimide [(b) and (d)] films. The polyamic acid is 2.18 μm thick, consists of 47-at.% carbon, 35-at.% hydrogen, 7-at.% nitrogen, 11-at.% oxygen, and has a density of 1.28 g/cm^3. The polyimide film is 1.78 μm thick, consists of 55-at.% carbon, 26-at.% hydrogen, 7-at.% nitrogen, 12-at.% oxygen, and has a density of 1.44 g/cm^3.

polyamic acid and polyimide films was determined to be 1.29±0.02 g/cm^2 and 1.44±0.02 g/cm^2, respectively. The value of knowing these data is twofold: (1) the implosion dynamics can be more accurately modeled, and (2) significant changes in density and porosity can induce significant changes in the residual intrinsic stress that affects the survivability and ultimate strength of the material.

Summary

Two ion-beam techniques, Rutherford backscattering spectroscopy and nuclear resonance analysis of hydrogen, used in conjunction, provide an accurate method for analyzing the complete elemental composition of individual capsules. These data are used to interpret ICF data and to support the development of suitable targets. The strengths of these techniques are (1) they are absolute measurements that do not rely on external calibration to infer the composition of the substrate material, and (2) they provide depth-resolved information, essential data to confirm that the fabricated targets are what they were designed to be.

ACKNOWLEDGMENT

REFERENCES

1. S. A. Letts, D. W. Myers, and L. A. Witt, J. Vac. Sci. Technol. **19**, 739 (1981).

2. N. Abbas, ICF Target Component Fabrication and Technology Development Support, FY96 Year-End Review, San Diego, CA (October 1996).

3. Internal Confinement Fusion Target Component Fabrication and Technology Development Support, General Atomic's Annual Report to the U.S. Department of Energy, 1 October 1996–30 September 1997.

4. A. Antolak, ICF Target Component Fabrication and Technology Development Support, FY97 Year-End Review, San Diego, CA (October 1997).

5. J. R. Tesmer and M. A. Nastasi, eds. *Handbook of Modern Ion Beam Materials Analysis* (Materials Research Society, Pittsburgh, PA, 1995).

6. P. Bodo and M. Schott, Thin Solid Films **286**, 98 (1996).

7. J. F. Ziegler, J. P. Biersack, and U. Littmark, *The Stopping and Range of Ions in Solids*, The Stopping and Ranges of Ions of Matter, Vol. 1 (Pergamon Press, New York, 1985).

8. L. R. Doolittle, Nucl. Instrum. Methods Phys. Res. B **B9**, 334 (1985).

9. D. D. Meyerhofer, presented at the 25th European Conference on Laser Interactions with Matter (25th ECLIM), Formia, Italy, 4–8 May 1998.

10. E. L. Alfonso, S.-H. Chen, R. Q. Gram, and D. R. Harding, "Properties of Polyimide Shells Made Using Vapor Phase Deposition," to be published in the Journal of Materials Research.

11. E. L. Alfonso, S.-H. Chen, R. Q. Gram, D. R. Harding, and F. Y. Tsai, "Fabrication of Polyimide Shells by Vapor Phase Deposition for Use as ICF Targets," presented at the Target Fabrication Meeting, Jackson Hole, WY, 19–23 April 1998, and to be published in Fusion Technology.